Electronic Supplementary Material (ESI) for Journal of Materials Chemistry A.

Urchin-like $NiCo_2O_4$ Hollow Microspheres and $FeSe_2$ Microsnowflake for Flexible Solid-State Asymmetric Supercapacitor

Chenchen Ji,[1] Fuzhu Liu,[1] Liang Xu,[1] Shengchun Yang,[1,2]*

1 MOE Key Laboratory for Non-equilibrium Synthesis and Modulation of Condensed Matter, State Key Laboratory for Mechanical Behavior of Materials, Xi'an Jiaotong University, Xi'an, 710049, People's Republic of China.

2 Collaborative Innovation Center of Suzhou Nano Science and Technology, Suzhou Academy of Xi'an jiaotong University, 215000, Suzhou, People's Republic of China.

*Email: ysch1209@mail.xjtu.edu.cn, +86-29-82663034.

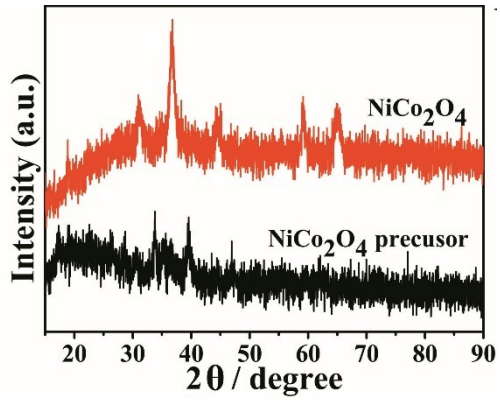

Fig.S1(a) XRD pattern of the $NiCo_2O_4$ UHMS precusor.

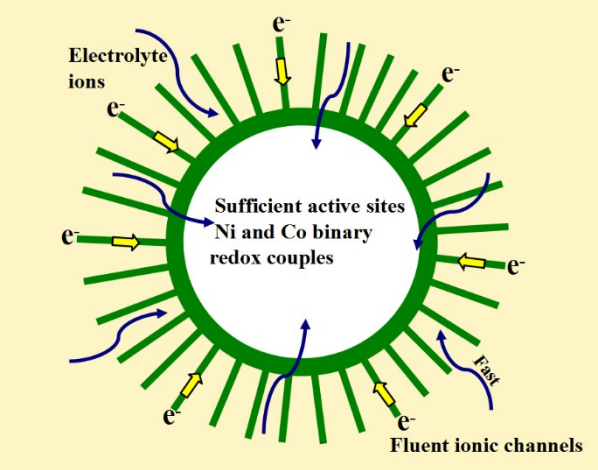

Fig.S2 Scheme for the advantages of this novel $NiCo_2O_4$ UHMS structure.

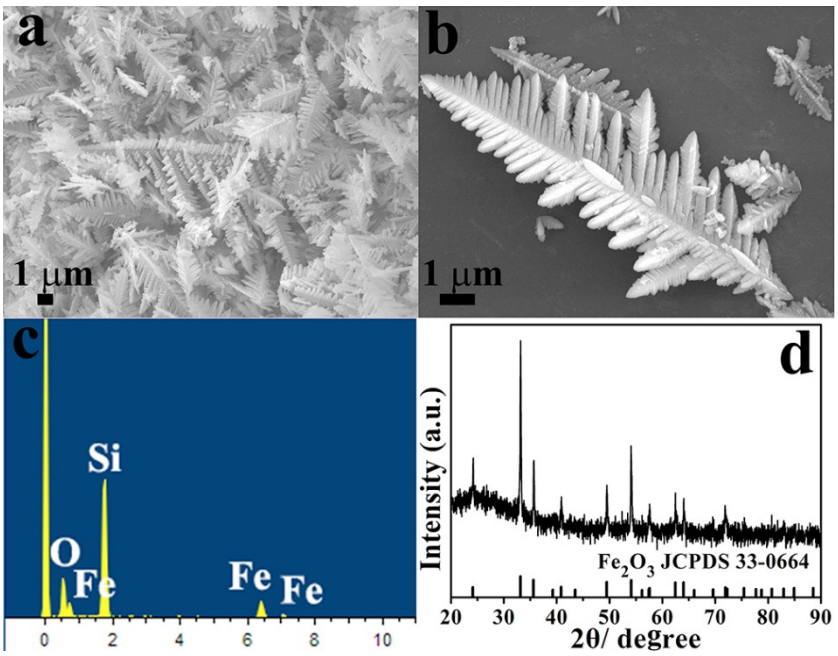

Fig.S3 (a-b) SEM images, (c) EDX spectrum and (d) XRD pattern of the Fe_2O_3 sample.

SEM images indicate that the element Se would react with Fe_2O_3 phase through an

ion-exchange process and form a more stable phase of $FeSe_2$. Fig.S4a-b show the morphology of the sample prepared under the same conditions for the $FeSe_2$ SF, except that the Se powder was not added. The micron-pine dendrite with some particles after the heating process were observed, and the obtained sample still maintain the orange color of Fe_2O_3. This means that the Fe_2O_3 phase was relatively stable in the oleylamine solution at high temperature. In contrast, the addition of Se powder noticeably altered the morphology of the Fe_2O_3 (Fig.3a-f). For the sample prepared by only adding the Se powder, fibers with smooth surfaces were observed, with occasional large particles located separately (Fig.S4c-d), which was totally different from the morphology of the original Se powder (Fig.S4d, inset). This results indicated that the element Se would reversibly thermally dissolve and recrystallize from the oleylamine solution, which bring about the formation of the fibers structure. If $FeCl_3$ was used as the Fe source, particles assembled by rectangle units without curly structure were obtained, which indicated that only the Fe_2O_3 precusor without the Fe-ions can lead the formation of such micron-snowflake and the curly structures. Based on the above results, it indicates that element Se is relative active in the oleylamine during the heating process, which could react with the Fe_2O_3 through an anion exchange process to form the more stable phase of $FeSe_2$.

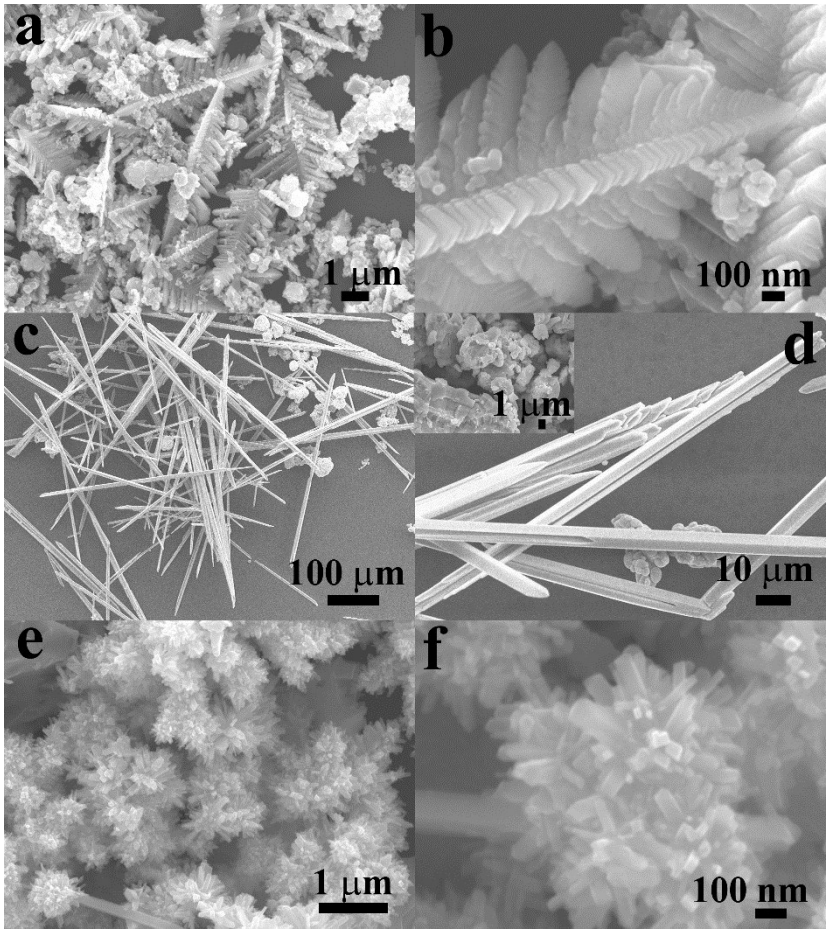

Fig.S4. (a-b) SEM images of the sample prepared under the same conditions for the $FeSe_2$ SF, except that the element Se was not added. (c-d) SEM images of the sample prepared under the same conditions for the $FeSe_2$ SF, except that the Fe_2O_3 was not added. (e-f) SEM images of the sample prepared by using $FeCl_3$ as the Fe source.

To reveal the evolution process from Fe_2O_3 micron-pine dendrite to $FeSe_2$ micron-snowflake architecture, time-dependent experiments were carried out. SEM images for the samples obtained at different reaction time is shown in Fig.S5. During the initial 20 min of accelerating heating from room temperature to 100 °C, the obtained sample still maintains the micron-pine dendrite structure (Fig.S5a and b), which indicated that no exchange-reaction was occurred at this stage. After 30 min of accelerating heating from room temperature to 120 °C (Fig.S5c and d), few snowflakes formed that were grown on the surface of the micron-pine dendrite. When the accelerating heating time was reached to 50 min (Fig.S5c and d), more and more snowflake structures formed with

dissolution of the Fe_2O_3 precusor, and the corroded pine dendrite can be clearly seen in the SEM images (Fig.S5e-h). When the reaction temperature reached to 200 °C, well defined snowflake structures were formed until totally dissolution of the pine dendrite precusor (Fig.S5i-t). On the basis of our analyses, it can be inferred that this anion exchange reaction accompanied by a morphology reconstruction process in our reaction system. Fe_2O_3 is thermodynamically less stable than that of the $FeSe_2$ in the oleylamine solution. The thermally soluble element Se could react with the Fe_2O_3 through an anion exchange reaction to form the $FeSe_2$ phase by a morphology reconstruction.

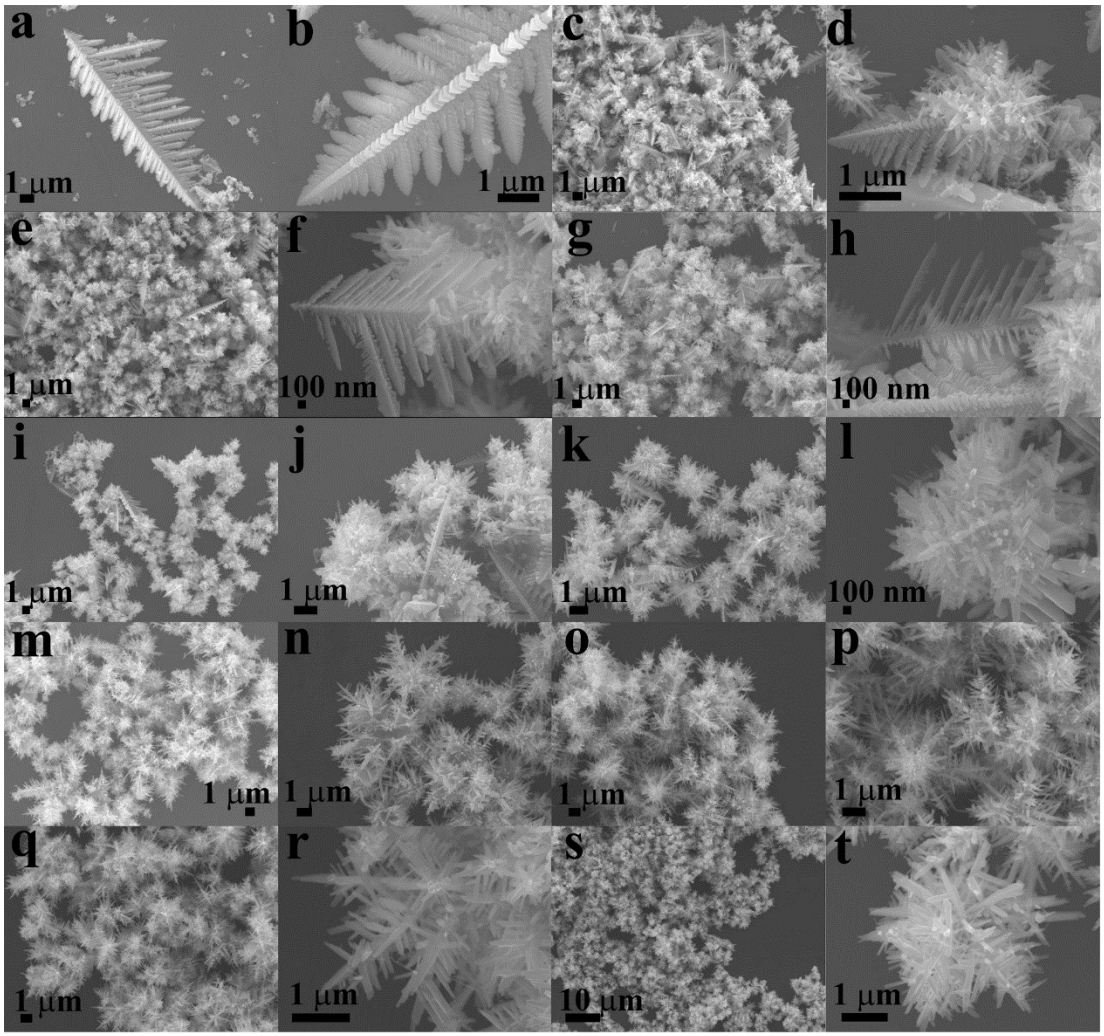

Fig.S5. SEM images of the evolution from Fe_2O_3 micron-pine dendrite structure to $FeSe_2$ micron-snowflake architecture prepared under different reaction time: after (a-b) 20 min; (c-d) 30 min; (e-f) 50 min; and (g-h) 60 min of accelerating heated from room temperature, and after (i-j) 10 min, (k-l) 20 min, (m-n) 30 min, (o-p) 40 min, (q-r) 50 min, and (s-t) 1 h at 200 °C.

Table SI. The specific capacitance comparison of other ASC full cells

Serial no.	ASC	Electrolyte	Specific capacitance	Ref
1	carbon//nickel oxide	6 M KOH	37 F g^{-1}	1
2	AC//Co_3O_4 NSs-rGO	2 M KOH	46 F g^{-1}	2
3	GHCS//GHCS-MnO_2	1 M Na_2SO_4	24.5 F g^{-1}	3
4	GH//MnO_2-NF	0.5 M Na_2SO_4	41.7 F g^{-1}	4
5	AC//AC-MnO_2	0.5 M Na_2SO_4	23.1 F g^{-1}	5
6	AC//Ni-Co oxide	1 M KOH	60 F g^{-1}	6
7	CNFs//Ni_3S_2/CNFs	2 M KOH	56.6 F g^{-1}	7
8	rGO//NiO	1 M KOH	50 F g^{-1}	8
9	AC // $NiCo_2O_4$ NSs@HMRAs	1 M KOH	70.04 F g^{-1}	9
10	$FeSe_2$//$NiCo_2O_4$	2 M KOH	71.7 F g^{-1}	Our work

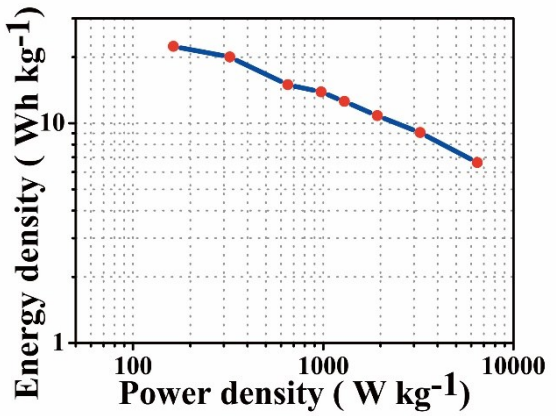

Fig.S6 Ragone plot of the fabricated (-)$FeSe_2$//$NiCo_2O_4$(+) ASC device.

Fig.S7 Optical photographs of the flexible current collector made from Scotch tape with good electrical conductivity.

Reference:

[1] Wang, D. W.; Li, F.; Cheng, H. M. Hierarchical Porous Nickel Oxide and Carbon as Electrode Materials for Asymmetric Supercapacitor. *J. Power Sources* **2008**, *185*, 1563-1568.

[2] Yuan, C.; Zhang, L.; Hou, L.; Pang G.; Oh, W. H. One-Step Hydrothermal Fabrication of Strongly Coupled Co_3O_4 Nanosheets-Reduced Graphene Oxide for Electrochemical Capacitors. *RSC Adv.* **2014**, *4*, 14408-14413.

[3] Lei, Z.; Zhang, J.; Zhao, X. S. Ultrathin MnO_2 Nanofibers Grown on Graphitic Carbon Spheres as High-Performance Asymmetric Supercapacitor Electrodes. *J. Mater. Chem.* **2012**, *22*, 153-160.

[4] Gao, H.; Xiao, F.; Ching, C. B.; Duan, H. High-Performance Asymmetric Supercapacitor Based on Graphene Hydrogel and Nanostructured MnO_2. *ACS Appl. Mater. Interfaces* **2012**, *4*, 2801-2810.

[5] Wang, Y. T.; Lu, A. H.; Zhang, H. L.; Li, W. C. Synthesis of Nanostructured Mesoporous Manganese Oxides with Three-Dimensional Frameworks and Their Application in Supercapacitors. *J. Phys. Chem. C* **2011**, *115*, 5413-5421.

[6] Tang, C.; Tang, Z.; Gong, H. Hierarchically Porous Ni-Co Oxide for High Reversibility Asymmetric Full-Cell Supercapacitors. *J. Electrochem. Soc.* **2012**, *159*, A651-A656.

[7] Yu, W.; Lin, W.; Shao, X.; Hu, Z.; Li, R.; Yuan, D. High Performance Supercapacitor Based on Ni_3S_2/Carbon Nanofibers and Carbon Nanofibers Electrodes Derived from Bacterial Cellulose. *J. Power Sources* **2014**, *272*, 137-143.

[8] Luan, F.; Wang, G.; Ling, Y.; Lu, X.; Wang, H.; Tong, Y.; Liu, X. X.; Li, Y. High Energy Density Aasymmetric Supercapacitors with a Nickel Oxide Nanoflake Cathode and a 3D Reduced Graphene Oxide Anode. *Nanoscale* **2013**, *5*, 7984-7990.

[9] Xue-Feng Lu, Dong-Jun Wu, Run-Zhi Li, Qi Li, Sheng-Hua Ye, Ye-Xiang Tong, Gao-Ren Li. Hierarchical $NiCo_2O_4$ nanosheets@hollow microrod arrays for high-performance asymmetric supercapacitors. J. Mater. Chem. A, 2014, 2, 4706-4713.